

to appear in the January 2001 issue of the PASP

HST Color-Magnitude Data for Globular Clusters: I. Transformations Between STIS LP Magnitudes and WFPC2 F606W and F814W Magnitudes¹

Mark L. Houdashelt, Rosemary F. G. Wyse

*Department of Physics & Astronomy, Johns Hopkins University,
3400 North Charles Street, Baltimore, MD 21218*

and

Gerard Gilmore

*Institute of Astronomy, University of Cambridge,
Madingley Road, Cambridge CB3 0HA, UK*

ABSTRACT

We present deep *Hubble Space Telescope* optical imaging observations of two Galactic globular clusters, 47 Tuc and M15, using the *Space Telescope Imaging Spectrograph* (STIS) longpass (LP) filter and the *Wide Field and Planetary Camera 2* (WFPC2) F606W and F814W filters. These globular clusters have very different metallicities ($[\text{Fe}/\text{H}] \sim -0.7$ dex for 47 Tuc, and $[\text{Fe}/\text{H}] \sim -2.2$ dex for M15), essentially spanning the metallicity distribution of the entire Milky Way globular cluster system, and were chosen to investigate the relationship between magnitudes in the non-standard STIS LP system and the better characterized WFPC2 magnitudes. We determine this relationship by combining our new STIS data with archival WFPC2 data, taking care to provide a robust and reliable transformation. Examining the 47 Tuc and M15 data separately, there is no evidence for a metallicity dependence in the transformation relations. This allows us to combine the data for both clusters, and also include the stars in the Small Magellanic Cloud that lie within the field of view of the 47 Tuc images, to determine final transformations that are valid for main sequence stars with colors in the range $0.3 \lesssim V_{606} - I_{814} \lesssim 1.8$. These final relations predict STIS magnitudes within 0.05 mag (1σ) of those measured for stars in both clusters. In an appendix, we discuss the differences between our empirical transformation relations and those predicted by synthetic photometry.

Subject headings: globular clusters: general — globular clusters: individual (NGC 104, NGC 7078) — Magellanic Clouds — stars: imaging — techniques: photometric

¹Based on observations with the NASA/ESA *Hubble Space Telescope*, obtained at the Space Telescope Science Institute, which is operated by AURA, Inc., under NASA contract NAS5-26555.

1. Introduction

We have obtained deep *Hubble Space Telescope* (HST) observations of the outer regions of two Galactic globular clusters, 47 Tuc (NGC 104) and M15 (NGC 7078), using the *Space Telescope Imaging Spectrograph* (STIS) and the *Near-Infrared Camera and Multi-Object Spectrometer* (NICMOS), as supporting observations for a project (GO 7419) with the scientific goal of determining the faint stellar luminosity function (LF) in the apparently dark-matter-dominated Ursa Minor dwarf spheroidal galaxy (UMi dSph). These data are supplemented by archival *Wide-Field and Planetary Camera 2* (WFPC2) observations of these clusters and were obtained to aid our understanding of the deep STIS data for the Ursa Minor galaxy. The UMi dSph is one of the few Galactic satellites which appears to have undergone a very short-lived episode of star formation; indeed, its stellar population is remarkably similar to that of a classical halo globular cluster such as M15, being old and metal-poor (Mateo 1998). Thus, a direct comparison between the luminosity functions of M15 and the UMi dSph is equivalent to a stellar mass function comparison and constrains the amount of baryonic dark matter in the UMi dSph (see Feltzing, Gilmore & Wyse 1999 and Wyse et al. 1999 for preliminary analyses that find remarkable similarity between the LFs of the UMi dSph, M15 and M92, another metal-poor halo globular cluster).

In this paper, we discuss the application of our multi-instrument photometry of 47 Tuc and M15 to the derivation of transformations from one photometric system to another. Here, we use aperture photometry of stars in these clusters to derive transformations between the WFPC2 data taken with the F606W and F814W filters and STIS photometry taken with the optical longpass (LP) filter, including an investigation of the possible existence of any metallicity dependence introduced by the broad STIS LP filter. Unless otherwise noted, we specify the sizes of all photometric apertures in terms of their radii (not their diameters) throughout this paper. In Section 2, we describe the observational data and their reduction. Section 3 discusses the photometry and how we selected the stars used in calculating the photometric transformations. Section 4 presents the resulting transformation equations, and further discussion of these results is given in Section 5. We summarize our conclusions in Section 6, and Appendix A describes the differences between our empirical transformation relations and the relations predicted by SYNPHOT. In a complementary paper, Beaulieu et al. (2000) derive similar calibrations from STIS LP and WFPC2 F555W and F814W observations of NGC 6553, a metal-rich ($[Fe/H] \sim -0.2$) and highly reddened ($E_{B-V} \sim 0.7$) globular cluster.

2. Observations and Data Reduction

For both 47 Tuc and M15, the pointing and orientation of HST were chosen so that the fields observed with STIS and NICMOS would lie within regions of these clusters for which archive WFPC2 images were available. Here, we discuss only the STIS and WFPC2 data; the NICMOS observations will be presented in a future paper. Table 1 summarizes the observational parameters

of the HST datasets that we used to obtain WFPC2 and STIS magnitudes of stars in 47 Tuc and M15. All of the data reduction was performed using standard STSDAS tasks within IRAF².

2.1. STIS

The STIS field for M15 was centered at $\alpha_{2000} = 21^{\text{h}} 29^{\text{m}} 42.^{\text{s}}43$, $\delta_{2000} = 12^{\circ} 11' 18.^{\text{s}}6$, a region $4.^{\prime}6$ (~ 65 r_c ; Harris 1996) from the cluster’s center that had been observed with WFPC2 as part of a GTO parallel program (HST proposal 5092). For 47 Tuc, STIS was also centered $4.^{\prime}6$ (~ 10 r_c ; Harris 1996) from the cluster’s center, at $\alpha_{2000} = 0^{\text{h}} 25^{\text{m}} 17.^{\text{s}}26$, $\delta_{2000} = -72^{\circ} 5' 36.^{\text{s}}9$, in a field which had been observed with WFPC2 as part of another GTO parallel program (HST proposal 5091) and also as part of the GO HST Medium-Deep Survey (HST proposal 5369).

The characteristics of STIS and the on-orbit performance of this instrument are described by Kimble et al. (1998). For all of the STIS observations of 47 Tuc and M15 discussed here, we used gain=4, CR-SPLIT=5, the STIS optical CCD, which consists of 1024×1024 pixels and has a plate scale of $0.^{\prime\prime}05071$ pixel $^{-1}$, and the optical longpass (LP) filter, which provides a rather flat throughput longwards of ~ 6000 Å to the $1\mu\text{m}$ limit (and reduces the STIS effective field of view to approximately $28'' \times 51''$). We will refer to magnitudes measured through this filter as I_{LP} magnitudes; these are non-standard magnitudes that we relate here to the more conventional WFPC2 systems.

Data reduction for the STIS observations of both clusters involved a simple recalibration of the images using the most up-to-date reference files and the IRAF task `calstis`. Figures 1 and 2 show the resulting STIS LP images of 47 Tuc and M15, respectively.

2.2. WFPC2

WFPC2 consists of four 800×800 pixel CCDs – the Planetary Camera (PC), which has a plate scale of $0.^{\prime\prime}0455$ pixel $^{-1}$, and three wide-field (WF) CCDs, each having an $80'' \times 80''$ field of view ($0.^{\prime\prime}1$ pixel $^{-1}$). A general description of WFPC2 and its on-orbit performance is given by Trauger et al. (1994) and by Holtzman et al. (1995a). As Table 1 indicates, we used WFPC2 observations of 47 Tuc and M15 that were taken with the broad band F606W and F814W filters. The former is well approximated as a wide version of Johnson’s V-band filter and the latter produces magnitudes which are nearly equivalent to Cousins I-band magnitudes, so we will refer to magnitudes in the F606W and F814W filters as V_{606} and I_{814} , respectively.

The WFPC2 observations of M15 have been previously analyzed by De Marchi & Paresce

²IRAF is distributed by National Optical Astronomy Observatories, operated by the Association of Universities for Research in Astronomy, Inc., under contract with the National Science Foundation.

(1995a) and by Piotto, Cool, & King (1997). G. Piotto (private communication) kindly provided the V_{606} and I_{814} magnitudes and the WFPC2 coordinates of the M15 stars used by Piotto, Cool, & King (1997) in their determination of the luminosity function of this cluster. These data have a total integration time of 6050 sec in each of the F606W and F814W filters.

The WFPC2 data for 47 Tuc were taken from the HST Archive and recalibrated using the task `calwp2`, again adopting the most up-to-date reference files; a subset of these observations, those from HST proposal 5091, were previously analyzed by De Marchi & Paresce (1995b). The multiple WFPC2 images of 47 Tuc were combined using a basic shift-and-average technique. The pixel offsets between images were determined from the positions of 275 relatively bright, isolated stars and ranged from 0–42 pixels for the thirteen F606W images; the two F814W images were not offset with respect to one another. After aligning the images and scaling by the exposure times, the images in each filter were averaged, ignoring bad pixels determined from the CCD characteristics or flagged in the data quality files. The combined images, which had total integration times of 5530 sec in F606W and 730 sec in F814W, were then used for the WFPC2 photometry of 47 Tuc.

3. Photometry

All of the photometry was performed with tasks within the `daophot` package of IRAF. First, `daofind` was used to detect stars greater than 3.5σ above the background on each image. Stellar magnitudes were then calculated with `phot`, using a 2-pixel aperture and a sky annulus with an inner radius of $0.^{\circ}5$ and a width of $0.^{\circ}5$. Finally, multiaperture photometry of 40–50 bright, isolated stars was used with `mkapfile` to determine the aperture corrections needed to transform the 2-pixel magnitudes to those appropriate for a $0.^{\circ}5$ aperture; the resulting aperture corrections are given in Table 2.

3.1. STIS Photometry

For the STIS LP observations, 1307 and 1041 objects were detected by `daofind` in the 47 Tuc and M15 images, respectively. The top panels of Figure 3 show the 1σ uncertainties in the measured (2-pixel aperture) I_{LP} magnitudes of these “stars” as a function of magnitude. The greater scatter in the 47 Tuc uncertainties is due to the larger number of image artifacts (diffraction spikes, etc.) seen in the 47 Tuc image (Figure 1) and detected as “stars” by `daofind`; these are eliminated in later processing and analysis of the data.

3.2. WFPC2 Photometry

As mentioned previously, the WFPC2 magnitudes of the M15 stars were provided by G. Piotto; the corresponding data reduction and photometric techniques, which differ somewhat from our methods (see Section 5), are discussed fully by Piotto, Cool, & King (1997). We utilized only their WF4 data because our STIS image of M15 falls entirely within its field of view.

For 47 Tuc, the WFPC2 data from the WF2 chip completely encompasses our STIS image, and `daofind` detected 4206 and 3886 “stars” on the combined WF2 F606W and F814W images, respectively. The bottom panels of Figure 3 show the 1σ uncertainties in the measured (2-pixel aperture) V_{606} and I_{814} magnitudes of these stars as a function of magnitude.

WFPC2 data have been shown to be subject to three effects that can produce systematic errors in the photometric magnitudes measured with this instrument: geometric distortion, charge transfer efficiency (CTE) effects, and the long-versus-short (LvS) anomaly. The geometric distortion of WFPC2 and the CTE effect are fully discussed by Holtzman et al. (1995a) and Holtzman et al. (1995b) and in the latest versions of the HST Data Handbook and the WFPC2 Instrument Handbook (Biretta et al. 2000); the latter two references also discuss the LvS anomaly. A brief description of each of these effects follows.

Geometric distortion causes the effective pixel size to be smaller at the edge of a WFPC2 chip than at its center, making the integrated magnitude of a star appear progressively fainter as it falls further from the center of the chip. For a CCD read out from top to bottom and left to right, the CTE effect causes a star to have a fainter measured magnitude when it falls near the top (and/or left-hand side) of one of the WFPC2 CCDs than when it falls near the bottom (and/or right-hand side) of the same chip. This is caused by charge trapping, i.e. loss of charge, as the signal from the star is transferred across the chip during readout. The CTE loss is greatest for faint stars with low background levels, and the top-to-bottom loss is generally larger than the left-to-right loss. For faint stars, the CTE effect has also become more pronounced with time. The LvS anomaly produces stellar magnitudes which are brighter in longer exposures, or more correctly, which appear brighter as their total count levels increase; its cause is currently unknown (and its existence has recently been questioned by Dolphin 2000).

We have not corrected the WFPC2 magnitudes of 47 Tuc for any of the three effects described above. Correcting for geometric distortion involves multiplying the WFPC2 image by a correction image before performing photometry (see the HST Data Handbook). However, since geometric distortion mainly affects stars lying near the edges of the WFPC2 chips, while our STIS frames tend to overlie the central part of the respective WF images and cover only about 22% of the field-of-view of a WF camera, we have ignored this correction. The latest correction algorithms for the CTE effect and the LvS anomaly are described by Whitmore, Heyer & Casertano (1999) and Casertano & Mutchler (1998), respectively, but each depends upon the total counts detected for a star and are thus exposure-time dependent and inapplicable to data made up of a combination of images having different exposure times. For this reason, and because the WFPC2 photometry of M15 was not

corrected for these two effects by Piotto, Cool, & King (1997), we have not corrected the WFPC2 magnitudes of the 47 Tuc stars for either the CTE effect or the LvS anomaly. Nevertheless, we have estimated how these two phenomena would affect our measured WFPC2 magnitudes and have used these estimates to limit the magnitude range over which we analyze our photometry; we will discuss these magnitude selection criteria further in Section 3.5.

3.3. Flight-System Magnitudes

We define a flight system magnitude, FMAG, similar to Holtzman et al. (1995b):

$$\text{FMAG} = -2.5 \times \log (\text{DN s}^{-1}) + \text{ZP} + 2.5 \times \log \text{GR}, \quad (1)$$

where DN are counts within a $0.^{\prime\prime}5$ aperture, ZP is the photometric zero point correction, and GR is the gain ratio used for the given CCD. Holtzman et al. (1995b) defined GR to be unity for WFPC2 observations made with `gain=14`; we define GR to be unity for STIS CCD observations made with `gain=1`. Table 2 lists the zero point corrections, gain ratios, and aperture corrections used here to put our 2-pixel aperture photometry onto the WFPC2 and STIS flight systems.

3.4. Matching Stars in F606W and F814W

The positions of 270 of the stars used to align the F606W images of 47 Tuc were used with the IRAF task `imagfe` to determine the coordinate transformation between the combined F606W and combined F814W images of 47 Tuc. Using this transformation, the coordinates of the stars detected in F814W were matched to those detected in F606W, accepting only those matches for which the predicted and measured positions agreed within 1.0 pixel. This produced a list of 2605 stars having both V_{606} and I_{814} magnitudes in the WF2 frame of 47 Tuc. The M15 data from Piotto, Cool, & King (1997) contained 3465 WF4 stars detected in both the F606W and F814W filters.

The top panels of Figures 4 and 5 show the resulting WFPC2 color-magnitude diagrams (CMDs) of these clusters; the magnitudes used in these figures have now been corrected to a $0.^{\prime\prime}5$ aperture. Figure 4 shows a tight main sequence for 47 Tuc, with the main-sequence turnoff occurring near the bright end of the data displayed there. A second sequence of stars is also visible in this figure, lying about 1 magnitude bluer than the 47 Tuc main sequence for $V_{606} > 22$; this is composed of main-sequence stars in the Small Magellanic Cloud (SMC), against which 47 Tuc is projected on the sky. Figure 5 shows a similarly well-defined main sequence for M15, with the main-sequence turnoff again appearing at the brightest magnitudes shown.

3.5. Selecting the Main-Sequence Stars

For the comparisons between the WFPC2 and STIS photometry of M15 and 47 Tuc, we restricted our analysis to stars that: 1) lie on the main sequences of these clusters, and 2) have photometry that has not been significantly affected by the CTE effect or by the LvS anomaly discussed in Section 3.2. Using the correction formula for the LvS anomaly given by Casertano & Mutchler (1998), we determined that the photometric magnitudes would become systematically too faint by about 0.1 mag at $V_{606} \sim 24.5$ and $I_{814} \sim 23$ for 47 Tuc and at $V_{606} \sim 25$ and $I_{814} \sim 24$ for M15. Thus, we applied these magnitude cuts to the WFPC2 data before determining which stars were main-sequence members; the magnitude bounds adopted for 47 Tuc and M15 are shown as dotted horizontal lines in the top panels of Figures 4 and 5, respectively. The boxes described by the solid lines in the top panels of Figure 4 surround the regions of the CMDs used to determine the location of the SMC main sequence. There are 2049 and 2057 stars lying between the V_{606} and I_{814} magnitude limits adopted for 47 Tuc, respectively; 143 of these stars lie within the SMC box in the V_{606} vs. V_{606} – I_{814} CMD, while only 71 lie within the analogous box in the I_{814} vs. V_{606} – I_{814} CMD. For M15, 1950 and 2043 stars lie within the chosen V_{606} and I_{814} bounds, respectively. We estimate that the CTE effect will cause the fluxes that we measure for the faintest stars used in the main-sequence fitting to be about 3% too faint (on average) while also introducing an additional scatter of about 0.03 mag in the WFPC2 magnitudes measured for the faintest stars.

After applying the magnitude cuts shown in Figures 4 and 5, we selected the main-sequence stars by fitting ridge lines to the remaining data using an iterative procedure. First, the stars were binned in 0.5 magnitude bins, and the median V_{606} – I_{814} color and mean magnitude were calculated in each bin. A fourth-order polynomial (second-order for the SMC) was fit to the median color as a function of magnitude, producing an equation for the main-sequence ridge line. Then, in each magnitude bin, the average color deviation from the ridge line was calculated, and a second-order relation was fit to the average color deviation as a function of magnitude. Using these two relations, we could then predict both the ridge-line color of every star in the CMD and the number of average deviations that the measured color of that star differed from the ridge-line color. To procure the final group of main-sequence stars in each cluster, we discarded all stars lying more than three average deviations from the ridge line and reiterated this procedure until no remaining stars were discarded. This algorithm was applied to both the V_{606} vs. V_{606} – I_{814} and I_{814} vs. V_{606} – I_{814} CMDs of each cluster, and the CMDs of the stars selected to be main-sequence members of 47 Tuc and M15 are shown in the bottom panels of Figures 4 and 5, respectively; the bottom panels of Figure 4 also shows the stars which lie on the main sequence of the background SMC. In the end, 1670, 120, and 1756 stars remained along the V_{606} vs. V_{606} – I_{814} main-sequence ridge lines of 47 Tuc, the SMC and M15, respectively. Likewise, the I_{814} vs. V_{606} – I_{814} ridge lines were defined by 1753, 61, and 1845 stars for 47 Tuc, the SMC and M15, respectively.

3.6. Matching Stars in WFPC2 and STIS

In exactly the same manner in which the F606W and F814W detections for 47 Tuc were matched, the stars detected with WFPC2 were paired with those seen in the STIS frames. Here, the positions of the stars used to calculate the I_{LP} aperture corrections were used to determine the coordinate transformations between the STIS images and the corresponding WFPC2 frames of each cluster, and stars which were located within 1.0 pixel of the expected position on the WFPC2 frames were matched to those detected with STIS. CMDs containing the stars detected in F606W, F814W and STIS LP are shown in the top panels of Figures 6 and 7 for 47 Tuc (and the SMC) and for M15, respectively. There were 657 stars detected in all three filters in 47 Tuc and the SMC; 796 stars were found in all three filters in M15. The bottom panels of Figures 6 and 7 show the subsets of the 47 Tuc and M15 stars, respectively, which also lie along the WFPC2 main sequences shown in the bottom panels of Figures 4 and 5; these samples are made up of 410, 19 and 467 stars in 47 Tuc, the SMC and M15, respectively, and are the stars that we used to determine the transformations between the V_{606} and I_{814} magnitudes measured with WFPC2 and the I_{LP} magnitudes measured with STIS.

4. Transformations Between the STIS and WFPC2 Systems

Before computing the transformations from V_{606} and I_{814} to I_{LP} , the flight magnitudes were corrected for extinction, using the reddening values for the given line of sight to each globular cluster; these reddening (taken from the on-line globular cluster catalog described by Harris 1996) and the resulting extinction corrections are listed in Table 2. The reddening-corrected color-color diagrams of the ridge-line stars detected in both WFPC2 filters and with the STIS LP filter are shown in Figure 8, where the 47 Tuc and SMC data are plotted in the left-hand panels as circular points and asterisks, respectively, and the M15 data are plotted in the right-hand panels.

For each instrument/filter combination, the appropriate extinction corrections were derived using SYNPHOT to calculate magnitudes as a function of reddening for the five spectra of K5 III stars listed in the Bruzual-Persson-Gunn-Stryker (BPGS) Spectrophotometry Atlas, adopting the reddening law of Cardelli, Clayton & Mathis (1989). At a given reddening, the magnitudes of the five stars were averaged and the difference between this mean magnitude and that measured at zero reddening was adopted for the extinction at that reddening. For the WFPC2 magnitudes, this procedure also involved averaging the extinctions derived from each of the three WF chips. The resulting extinction corrections appear to be quite dependable, as the A_{814} values differ by only ~ 0.001 mag from those determined independently by Holtzman et al. (1995b) and Hernandez, Gilmore & Valls-Gabaud (2000), and the A_{606} values differ by less than 0.010 mag from those estimated by Hernandez, Gilmore & Valls-Gabaud (2000).

We note that, in principle, extinction corrections can be nonlinear, complex functions of both the line of sight and the spectrophotometric properties of the source of interest. However, the

extinction levels in the 47 Tuc and M15 fields are sufficiently small that second-order effects are estimated to be much smaller than the random photometric errors. This is supported by alternative calculations of the extinction corrections, using the method described above but substituting the three spectra of G8 V stars from the BPGS Spectrophotometry Atlas for the spectra of the K5 giants. The corresponding extinction values are systematically higher than those adopted here, but the differences are $\lesssim 0.01$ mag in each of the three filters considered.

In deriving transformations between the WFPC2 and STIS photometric systems, we have considered two questions. First, are the transformations metallicity-dependent? Second, what is the functional form of the transformations? To address the latter question, we have performed both linear and quadratic least-squares fitting with iterative 3σ rejection, so the transformation relations take the general form:

$$I_{LP,0} = m_0 + ZP + a \times (V_{606} - I_{814})_0 + b \times (V_{606} - I_{814})_0^2 \quad (2)$$

where m_0 is the extinction-corrected WFPC2 magnitude, either $V_{606,0}$ or $I_{814,0}$, and ZP is the zero point of the fit.

If metallicity affects the color transformations, then we would expect the color-color relations of 47 Tuc and M15 to differ. This is indeed the case when linear relations are fit to the entire samples of the 47 Tuc and M15 ridge-line stars; these fits are shown as dashed lines in Figure 8, and the open points in this figure are the data thrown out by the iterative, 3σ rejection during the fitting. The coefficients of the dashed relations are listed in the uppermost section of Table 3, where it can be seen that both the zero points and the intercepts of the fits to these particular M15 and 47 Tuc photometric data differ by more than 3σ .

Does this imply that there is a metallicity dependence in the color transformations? Not necessarily. Due to the different metallicities and distance moduli of these two clusters, the range of $V_{606} - I_{814}$ colors which our selection criteria allow are not the same in each. As Figure 8 shows, the 47 Tuc ridge-line stars have $0.6 \lesssim V_{606} - I_{814} \lesssim 1.8$, while those in M15 have $0.3 \lesssim V_{606} - I_{814} \lesssim 1.0$. The M15 data extends to bluer colors because M15, with $[Fe/H] = -2.25$ (Harris 1996), is more metal-poor than 47 Tuc, which has $[Fe/H] = -0.76$ (Harris 1996). However, since the apparent distance modulus of M15 is ~ 2 magnitudes greater than that of 47 Tuc, the limiting magnitude of the STIS observations, coupled with the magnitude limits that we apply to the WFPC2 data, allows the 47 Tuc stars to extend to much redder $V_{606} - I_{814}$ colors than those in M15. The significance of these color range differences is that any curvature or break in slope of the true transformation relations could affect the linear fits to the two clusters differently. Thus, we must compare stars of similar color in 47 Tuc and M15 to look for metallicity effects.

Considering only the stars with $0.6 \leq V_{606} - I_{814} \leq 1.0$ in each cluster (those lying between the dotted, vertical lines in Figure 8), linear least-squares fits produce the relations shown as solid lines in Figure 8. The middle section of Table 3 shows that these new transformation relations for 47 Tuc

and M15 now differ at only the 1σ level. This improved agreement is caused by the substantially different fit for the color-restricted set of 47 Tuc stars than for the entire 47 Tuc sample; the M15 transformations do not change appreciably when the color boundaries are applied. Thus, metallicity effects are apparently unimportant in the transformation relations, and either the true transformations contain higher-order terms, or there is a change in slope at some color redder than $V_{606}-I_{814} = 1.0$.

Since there is no obvious sudden change in slope of the 47 Tuc color-color data at any color, higher-order fits are suggested. We have chosen to represent the WFPC2-to-STIS transformation equations by quadratic, least-squares fits. The fact that there is no metallicity dependence also allows us to combine all of the 47 Tuc, SMC and M15 data. The final transformations are illustrated in Figure 9, where the 47 Tuc, SMC and M15 stars are shown as circles, triangles and squares, respectively, and the quadratic fits are the solid curves drawn there. For clarity, we have not plotted the stars rejected during the fitting. The coefficients of these transformation relations are listed in the bottom section of Table 3.

Figure 10 shows the differences between the I_{LP} magnitudes measured for the 47 Tuc/SMC stars (left-hand panels) and the M15 stars (right-hand panels) and the magnitudes predicted by the quadratic transformation relation shown in the bottom panel of Figure 9 as functions of both V_{606} magnitude (top panels) and color (bottom panels). Here, the globular cluster stars are shown as filled points, and the SMC stars are asterisks; we have again omitted the stars rejected during the least-squares fitting. From this figure, it is apparent that the transformation relations generally predict I_{LP} magnitudes for the 47 Tuc and M15 stars within 0.05 mag (1σ) of those measured, with no systematic offset. However, the predicted I_{LP} magnitudes of the SMC stars, while also being good to about 0.05 mag, may be systematically ~ 0.05 mag too bright.

5. Discussion

We have argued that the differences between the linear fits to the complete samples of 47 Tuc and M15 color-color data shown in Figure 8 are due to the presence of a higher-order term in the “true,” metallicity-independent transformation relations. Here, we discuss some other effects which could also produce this outcome and explain why we feel that these are less important.

One possible source of differential systematic errors in the photometry is the different methodologies used to measure the WFPC2 magnitudes of 47 Tuc and M15. While both we and Piotto, Cool, & King (1997) performed aperture photometry, Piotto, Cool, & King (1997) used point-spread functions (PSFs) to first subtract nearby neighbors, which should improve the measured magnitudes, especially for the faintest stars. In addition, PSF-fitting allows the removal of spurious stellar detections (e.g. background galaxies, bad pixels) through various goodness-of-fit selection criteria, such as χ^2 and sharpness. However, since the 47 Tuc and M15 fields observed here are not particularly crowded, the photometric improvements produced by PSF-fitting are only expected to

be significant at the faintest magnitudes. Our use of magnitude cutoffs for the WFPC2 data and our exclusion of objects which do not lie along the cluster main-sequence ridge lines have likely minimized any differences caused by the photometric algorithms employed.

Likewise, the magnitude cutoffs that we have adopted should preclude any significant biases in the photometry due to incompleteness of the WFPC2 data. For the WF3 observations of M15, Piotto, Cool, & King (1997) estimated their data to be 93% complete at $V_{606}=25$ and 92% complete at $I_{814}=24$; these levels should be approximately the same for the WF4 data, for which De Marchi & Paresce (1995a) give a completeness level of 92% at $I_{814}=24$ and $I_{814}-V_{606}\sim 1$. We also expect the WF2 image of 47 Tuc to be more than 90% complete at the magnitude cutoffs used here. Although De Marchi & Paresce (1995b) estimated their WF2 completeness level to be only $\sim 80\%$ at $I_{814}=23$ and $I_{814}-V_{606}\sim 1.65$, this incompleteness was dictated by their F606W data. We use a much more extensive set of F606W observations than they did, so our completeness level will be determined by the F814W data, which De Marchi & Paresce (1995b) show to be $\sim 80\%$ complete one full magnitude fainter than our I_{814} cutoff.

Could the documented complications with WFPC2 photometry be the cause of the different linear transformation relations derived from the complete samples of 47 Tuc and M15 ridge-line stars? As discussed previously, the WFPC2 magnitudes in both clusters will be systematically too faint (about 3% on average) due to the CTE effect, but the differential effect between the two clusters should be negligible. The LvS anomaly, on the other hand, while also causing the WFPC2 magnitudes to be systematically too faint, will become increasingly important as the magnitudes become fainter. To first order, the errors in V_{606} and I_{814} will offset one another, so the $V_{606}-I_{814}$ colors will not be as greatly affected as the $V_{606}-I_{LP}$ and $I_{LP}-I_{814}$ colors will be. While we have attempted to compensate for the LvS anomaly through the magnitude limits that we have applied to the WFPC2 data, the 47 Tuc and M15 stars will still have $V_{606}-I_{LP}$ colors which are progressively too red and $I_{LP}-I_{814}$ colors which are progressively too blue as fainter stars are considered. This will introduce a slight bit of curvature in the color-color relations shown in Figure 8 and could potentially account for the differing transformation relations derived for the two clusters. However, this “curvature” will not occur at the same color in 47 Tuc and M15 (because of their differing distances and metallicities) and therefore should affect the fits derived from the color-restricted samples of their members as well. Since this is not seen, we do not expect that the CTE effect and LvS anomaly make significant contributions to the resulting transformation equations.

We have quantified this further by performing photometry on the longest-exposure F606W and I814W images of 47 Tuc listed in Table 1. We then used the algorithms suggested by Whitmore, Heyer & Casertano (1999) and by Casertano & Mutchler (1998) to correct the measured counts for the CTE effect and for the LvS anomaly, respectively, and calculated new magnitudes for these stars. Without applying any magnitude cutoff to these data, the same analysis procedure used for the combined images was adopted, resulting in a new determination of the 47 Tuc ridge-line stars. This set of data contains a smaller number of stars than the data resulting from the combined WFPC2 images because, even though it extends to slightly redder colors than the magnitude-

limited, combined data, most of the bright, blue main-sequence stars are no longer included because they are saturated in the 1500-sec F606W exposure.

Performing least-squares fits (with iterative 3σ rejection) to the corrected, single-image colors of the 47 Tuc ridge-line stars, the resulting linear and quadratic transformation relations have the coefficients listed in Table 4. Comparing these coefficients to the analogous fits from Table 3, we see that the linear fits have nearly identical slopes, while their intercepts differ by about 3%, as expected from the CTE effect. Thus, the magnitude cutoffs that we have applied to the combined-image data appear to have reasonably precluded the LvS anomaly from significantly biasing our results. This is reinforced by the 1σ agreement between the coefficients of the quadratic relations derived from the combined 47 Tuc, M15 and SMC data (Table 3) and those derived from the single-image 47 Tuc data alone (Table 4).

5.1. A Cautionary Note

Note that the transformation relations that we present are only valid for magnitudes in a $0.^{\prime\prime}5$ aperture. In particular, our transformations differ significantly from synthetic calculations, and we discuss this further in Appendix A, where we also describe a possible dependence of the I_{LP} aperture corrections on color. We especially encourage those who use SYNPHOT to calculate color-color transformations to read Appendix A and to use care when applying the SYNPHOT (infinite-aperture) results to infer observed magnitudes.

6. Summary

An important application of multiband photometry is the derivation of transformation relations between the corresponding photometric systems. In this paper, we have used our STIS observations of two Galactic globular clusters, 47 Tuc and M15, in combination with archival WFPC2 data of these clusters, to derive transformations which can be used to calculate STIS I_{LP} magnitudes from WFPC2 V_{606} and I_{814} data for main-sequence stars with colors in the range $0.3 \lesssim V_{606}-I_{814} \lesssim 1.8$ and metallicities in the range $-2.2 \lesssim [\text{Fe}/\text{H}] \lesssim -0.5$.

Considerable effort was spent to choose an optimal sample of stars to use in deriving the photometric transformations. This involved applying magnitude limits to the WFPC2 data to minimize the influences of the CTE effect and the long-vs.-short anomaly, each of which systematically affect WFPC2 photometry. We also used least-squares fitting to determine main-sequence ridge lines in the WFPC2 color-magnitude diagrams of each cluster and rejected those stars lying more than three average deviations from these ridge lines.

Comparing linear, least-squares fits to the color-color data of 47 Tuc and M15 over a similar range in $V_{606}-I_{814}$, we found that the coefficients of the fits differed by less than 1σ , indicating

that the “true” color-color relations have no metallicity dependence. We therefore combined the photometry of the 47 Tuc and M15 main-sequence stars (as well as a few stars in the SMC) and performed quadratic, least-squares fits to this combined data set to derive the suggested transformation relations. These can be used to predict I_{LP} magnitudes from V_{606} and I_{814} magnitudes, and the agreement between the predicted and measured I_{LP} magnitudes is generally good to 0.05 mag (1σ).

We thank G. Piotto for providing the WFPC2 photometry of M15 and for helpful suggestions regarding its use. We also express our gratitude to S. Feltzing, M. Bessell, H. Ferguson, J. Gallagher, B. Mobasher, N. Tanvir and T. Smecker Hane for their scientific insights and discussions. Support for this work was provided by NASA grant number GO-7419 from STScI, operated by AURA Inc, under NASA contract NAS5-26555.

A. Synthetic Transformation Relations

M. Bessell (private communication) has pointed out to us that his synthetic V_{606} , I_{814} , and I_{LP} photometry predicts different transformation relations than those that we present here. While his calculations of the transformations shown in Figure 9 verify that these relations are metallicity-independent and become nonlinear when stars redder than $V_{606}-I_{814} \sim 1.2$ are included, he finds that the coefficients of the synthetic relations differ significantly from those given in Table 3. In this appendix, we compare the results of SYNPHOT synthetic color calculations with our empirical data to evaluate two possible explanations for the observed differences: 1) use of an inappropriate STIS LP filter response function in SYNPHOT, and 2) a color dependence of the empirical I_{LP} aperture corrections.

A.1. SYNPHOT Calculations and the STIS LP Filter Response

We have used SYNPHOT to repeat Bessell’s investigation and have confirmed his basic finding that our empirical transformation relations differ from synthetic predictions. To do this, we calculated V_{606} , I_{814} , and I_{LP} magnitudes for stars no. 14–71 (B9–M8 dwarfs) of the BPGS Spectrophotometric Atlas within SYNPHOT. Ideally, we would expect only a constant offset between the observed and synthetic magnitudes because different aperture sizes apply for each – the SYNPHOT magnitudes are “infinite-aperture” magnitudes, while our reported magnitudes represent the light falling within a $0.^{\prime\prime}5$ aperture. However, the $V_{606}-I_{814}$ data should not be affected by the differing apertures; Holtzman et al. (1995b) estimate that an aperture correction of -0.1 mag is appropriate to adjust a $0.^{\prime\prime}5$ aperture magnitude to an infinite-aperture magnitude for any WFPC2 magnitude. The analogous aperture correction for I_{LP} magnitudes is unknown, so we have simply normalized the synthetic and empirical relations at $V_{606}-I_{814} = 0.3$, the approximate blue limit of our observational data, to more easily compare the slopes of the two relations differentially. The SYNPHOT calculations (open points) are compared to our final (normalized) transformation relations in the left-hand panels of Figure 11, where we show our empirical relations as solid lines spanning only the range of colors used in their derivation. The empirical and synthetic color-color relations differ significantly in slope, diverging by ~ 0.2 mag between $V_{606}-I_{814} = 0.3$ and $V_{606}-I_{814} = 1.8$.

Bessell has pointed out that the empirical transformations can be reproduced by synthetic color-color relations calculated with a modified STIS LP response function that has a significantly bluer effective wavelength than that reported in the STIS Instrument Handbook (Leitherer et al. 2000). To confirm this, we have performed SYNPHOT color calculations analogous to those described above but adopting the modified STIS LP filter response suggested by Bessell. The results are compared to our final transformation relations in the right-hand panels of Figure 11. In these panels of the figure, the empirical relations are the same as those which appear in the corresponding left-hand panels, but we have shifted the I_{LP} magnitudes calculated with the modified filter response to normalize them with our relations at $V_{606}-I_{814} = 0.3$, since the I_{LP} zero point for the modified

filter response will differ from that which we have adopted (Table 2). The normalized, synthetic colors computed with the modified LP filter response are quite similar to those observed over the entire range of colors used in deriving our transformation relations.

To give the reader a feel for the degree to which the STIS LP filter response would have to be modified to reproduce our empirical transformations, Figure 12 compares the STIS LP filter response tabulated in the STIS Instrument Handbook for Cycle 10 (Leitherer et al. 2000; dotted line) to that suggested by Bessell (2000, private communication; solid line). The transmission profile of the STIS LP filter is thought to be well-determined (H. Ferguson 2000, private communication), so any possible discrepancy between the tabulated response function and the “true” one would have to be due to a fairly dramatic change in some other component of the optical system (e.g., degradation of the CCD sensitivity at longer wavelengths) to change the filter response to the extent shown in Figure 12.

A.2. Aperture Corrections

The PSF of the STIS CCD is known to vary with wavelength, exhibiting an increasingly pronounced halo at wavelengths longer than about 7500 Å due to the scattering of light within the CCD (Leitherer et al. 2000); the red light in the PSF can be scattered to as much as 5'' from the PSF center. Therefore, the slopes of our transformation relations may differ from the SYNPHOT predictions because the fraction of light scattered to radii greater than 0.1'' differs for the red and blue cluster stars that we have observed. If this is the case, we would need to apply larger aperture corrections to the magnitudes of the red stars than those used for the bluer stars to reproduce the SYNPHOT calculations.

We have looked at the behavior of the I_{LP} aperture corrections for stars of different $V_{606}-I_{814}$ color by calculating magnitudes as a function of aperture radius for: 1) the stars in 47 Tuc that belong to the sample used to derive our transformation relations, 2) three bright PSF calibration stars for which HST archive STIS LP observations were available, and 3) Tiny Tim PSFs generated for dwarf stars of differing spectral types. Note that the Tiny Tim PSFs do not include the extended halo due to scattered light, so they will give only a baseline prediction for aperture corrections as a function of color.

The calibration stars (and HST proposals from which the archive STIS LP data were taken) are GRW +70 5824, a white dwarf (HST proposal 8422), SAO 255271, an F8 star (HST proposal 8842), and BD -11 3759, an M4 star (HST proposal 8422). Since no WFPC2 observations exist for these stars, their $V_{606}-I_{814}$ colors were derived from the following sources, using transformations from Holtzman et al. (1995b) as needed to convert from $V-I$ to $V_{606}-I_{814}$: 1) $V_{606}-I_{814} \sim -0.1$ for GRW +70 5824 from Figure 6 of Holtzman et al. (1995b), 2) $V_{606}-I_{814} \sim 0.5$ for SAO 255271 from an average of the SYNPHOT colors of F8 dwarfs in the BPGS Spectrophotometric Atlas, and 3) $V_{606}-I_{814} \sim 2.0$ for BD -11 3759 from an observed $(V-I)_C$ color (Leggett 1992). The Tiny Tim

PSFs were derived from the following stars (and their spectral types) in the BPGS Atlas: star 14 (A0 V), star 41 (F8 V), star 53 (G8 V), star 65 (K7 V), and star 68 (M3 V); the $V_{606}-I_{814}$ colors of these stars were calculated with SYNPHOT.

We first searched for a color dependence in the aperture corrections that we have applied to our 2-pixel magnitudes of the 47 Tuc stars to convert them to magnitudes in a $0.^{\prime\prime}5$ aperture. To increase the number of cluster stars for which $0.^{\prime\prime}5$ magnitudes could be measured, we calculated an empirical PSF based upon 55 stars in the 47 Tuc image. We then used this PSF to subtract all of the stars from the image except the star of interest before measuring its magnitude. The resulting aperture corrections, shown as open circles in Figure 13, exhibit substantial scatter for the reddest stars but do not show an obvious trend with color. However, the HST calibration stars hint that the aperture corrections may be larger for redder stars; these stars are shown as filled points in Figure 13. Measuring magnitudes in exactly the same manner described in Section 3.1, the two blue HST calibration stars (GRW +70 5824 and SAO 255271) have aperture corrections of -0.466 and -0.444 mag, respectively, which are in accord with our estimate (Table 2). The aperture correction for BD -11 3759, however, is about 0.1 mag greater than this. This indicates that the color sensitivity of the aperture corrections listed in Table 2 is weak at most and is insufficient to explain the empirical/SYNPHOT differences. The Tiny Tim PSFs infer that about 0.05 mag of the different aperture corrections for the red and blue HST calibration stars is due to effects other than the halo produced by scattered red light.

Of course, to compare observed magnitudes to SYNPHOT magnitudes, we should measure magnitudes in an aperture large enough to contain all of the light of a star. This is impossible to do in practice, so we have approximated infinite-aperture magnitudes by magnitudes measured in a $5''$ aperture. Unfortunately, we could not measure such magnitudes for any of the 47 Tuc stars, even after the other stars were subtracted from the image, because there was not a single star in the 47 Tuc image which did not contain at least one bad pixel within its $5''$ aperture. However, we were able to measure such magnitudes for two of the HST calibration stars, SAO 255271 and BD -11 3759, which differ in $V_{606}-I_{814}$ color by about 1.5 mag, and for the Tiny Tim PSFs, using an aperture with a radius of $5''$ and a sky annulus having an inner radius of $5''$ and a width of $0.^{\prime\prime}5$. For the two calibration stars, the corrections needed to transform magnitudes measured in a $0.^{\prime\prime}1$ aperture to those in a $5''$ aperture differ by about 0.17 mag, which is approximately the difference between the empirical and synthetic transformation relations between $V_{606}-I_{814} = 0.3$ and $V_{606}-I_{814} = 1.8$, the red end of the observational data used to derive the empirical relations. The Tiny Tim PSFs again indicate that all but 0.05 mag of this difference is due to the scattered-light halo of the PSF.

In conclusion, we cannot exclude the possibility that the differences between the slopes of the empirical and SYNPHOT transformation relations is due to a color dependence in the aperture corrections needed to transform the observed magnitudes to infinite-aperture magnitudes such as those computed with SYNPHOT. Thus, the extent that the STIS LP filter response may differ from that tabulated in the STIS Instrument Handbook for Cycle 10 (Leitherer et al. 2000) cannot

be determined from the datasets that we have analyzed. A more detailed study of the globular cluster fields using PSF-fitting could potentially prove illuminating but would be complicated by the dependence of the PSF shape on color and on position on the STIS CCD. Further investigation of the reasons for the differences between the empirical and synthetic transformation relations is required (and highly encouraged) but is beyond the scope of the present paper.

REFERENCES

Beaulieu, S. F., Gilmore, G., Elson, R. A. W., Johnson, R. A., Santiago, B., Sigurdsson, S., & Tanvir, N. 2000, AJ, submitted

Biretta, J. A., et al. 2000, WFPC2 Instrument Handbook, Version 5.0 (Baltimore: STScI)

Cardelli, J. A., Clayton, G. C., & Mathis, J. S. 1989, ApJ, 345, 245

Casertano, S., & Mutchler, M. 1998, Instrument Science Report WFPC2 98-02, STScI

De Marchi, G., & Paresce, F. 1995, A&A, 304, 202

De Marchi, G., & Paresce, F. 1995, A&A, 304, 211

Dolphin, A. E. 2000, PASP, 112, 1397

Feltzing, S., Gilmore, G. & Wyse, R. F. G. 1999, ApJ, 516, L17

Harris, W. E. 1996, AJ, 112, 1487

Hernandez, X., Gilmore, G., & Valls-Gabaud, D. 2000, MNRAS, 317, 831

Holtzman, J., et al. 1995a, PASP, 107, 156

Holtzman, J., Burrows, C. J., Casertano, S., Hester, J. J., Trauger, J. T., Watson, A. M., & Worthey, G. 1995b, PASP, 107, 1065

Kimble, R. A., et al. 1998, ApJ, 492, L83

Leggett, S. K. 1992, ApJS, 82, 351

Leitherer, C., et al. 2000, STIS Instrument Handbook, Version 4.0 (Baltimore: STScI)

Mateo, M. 1998, ARA&A, 36, 435

Piotti, G., Cool, A. M., & King, I. R. 1997, AJ, 113, 1345

Trauger, J. T., et al. 1994, ApJ, 435, 3L

Whitmore, B., Heyer, I., & Casertano, S. 1999, PASP, 111, 1559

Wyse, R. F. G., Gilmore, G., Feltzing, S., & Houdashelt, M. L. 1999, in ASP Conf. Ser. 193, The Hy-Redshift Universe: Galaxy Formation and Evolution at High Redshift, ed. A. J. Bunker & W. J. M. van Breugel (San Francisco: ASP), 181

Table 1. HST Datasets

Star Cluster	HST Instrument	HST Filter	HST Proposal	Observation Date	Exposure Time	HST Dataset
47 Tuc	WFPC2	F606W	5369	1994 Nov 11	1500.0	u26kbj01t
				1994 Nov 11	600.0	u26klr01t
				1994 Nov 11	300.0	u26kp701t
				1994 Nov 11	300.0	u26kp801t
				1994 Nov 11	300.0	u26kp901t
				1994 Nov 11	300.0	u26kpa01t
				1994 Nov 11	300.0	u26kpb01t
				1994 Nov 11	300.0	u26kqh01t
				1994 Nov 11	300.0	u26kqi01t
				1994 Nov 11	300.0	u26kqj01t
			5091	1994 Nov 11	300.0	u26kqk01t
				1994 Nov 11	230.0	u27z0301t
				1994 Nov 11	500.0	u27z2t01t
		F814W	5091	1994 Nov 11	230.0	u27z0302t
				1994 Nov 11	500.0	u27z2t02t
	STIS	LP	7419	1997 Oct 13	1290.0	o488a0010
M15	WFPC2	F606W	5092 ^a	1994 Jun 17	350.0	u2801h01t
				1994 Jun 17	500.0	u2803701t
				1994 Jun 17	600.0	u2803q01t
				1994 Jun 17	700.0	u2804d01t
				1994 Jun 17	799.5	u2804z01t
				1994 Jun 17	900.0	u2805j01t
				1994 Jun 17	1000.0	u2806101t
				1994 Jun 17	1200.0	u2806l01t
		F814W	5092 ^a	1994 Jun 17	350.0	u2801h02t
				1994 Jun 18	500.0	u2803702t
				1994 Jun 17	600.0	u2803q02t
				1994 Jun 17	700.0	u2804d02t
				1994 Jun 17	800.0	u2804z02t
				1994 Jun 17	900.0	u2805j02t
				1994 Jun 17	1000.0	u2806102t
				1994 Jun 17	1200.0	u2806l02t
	STIS	LP	7419	1998 Aug 16	1200.0	o488b9010

^aPhotometry provided by G. Piotto (private communication); see Piotto, Cool & King (1997) for details regarding the data reduction.

Table 2. Reddening, Aperture and Zero Point Corrections

Star Cluster	E(B-V) ^a	Instrument	Filter	A_{λ} ^b	Aperture Correction	Gain Ratio	Zero Point Correction	Zero Point Source
47 Tuc	0.04	WFPC2	F606W	0.109	−0.193	2.003	22.084	1
			F814W	0.074	−0.241	2.003	20.839	2
		STIS	LP	0.083	−0.465	0.250	25.868 ^c	3
M15	0.10	WFPC2	F606W	0.273	...	1.955	22.089	4
			F814W	0.184	...	1.955	20.840	4
		STIS	LP	0.208	−0.453	0.250	25.868 ^c	3

^aHarris 1996.

^bExtinction in the corresponding magnitude (see text).

^cEquivalent zero point in AB magnitudes is 25.279.

References. — (1) Table 9 of Holtzman et al. 1995b; (2) Table 6 of Holtzman et al. 1995b; (3) H. Ferguson, private communication; (4) G. Piotto, private communication.

Table 3. Transformation Equation Coefficients for Combined-Image Data^a

Data Set	V ₆₀₆ –I ₈₁₄	m ₀	ZP	σ	a	σ	b	σ	n
M15	all	I ₈₁₄	0.958	0.011	0.513	0.013	457
		V ₆₀₆	0.958	0.011	-0.487	0.013	457
47 Tuc	all	I ₈₁₄	1.023	0.009	0.423	0.007	380
		V ₆₀₆	1.023	0.009	-0.577	0.007	380
M15	0.6–1.0	I ₈₁₄	0.987	0.024	0.481	0.028	340
		V ₆₀₆	0.987	0.024	-0.519	0.028	340
47 Tuc	0.6–1.0	I ₈₁₄	0.982	0.018	0.466	0.023	86
		V ₆₀₆	0.982	0.018	-0.534	0.023	86
All	all	I ₈₁₄	0.924	0.014	0.633	0.027	-0.095	0.012	848
		V ₆₀₆	0.924	0.014	-0.367	0.027	-0.095	0.012	848

^a $I_{LP} = m_0 + ZP + a \times (V_{606} - I_{814}) + b \times (V_{606} - I_{814})^2$

Table 4. Transformation Equation Coefficients for Single-Image Data^a

Star Cluster	V ₆₀₆ –I ₈₁₄ Color Range	m ₀	ZP	σ	a	σ	b	σ	n
47 Tuc	all	I ₈₁₄	1.059	0.017	0.429	0.012	347
		V ₆₀₆	1.059	0.017	-0.571	0.012	347
47 Tuc	all	I ₈₁₄	0.925	0.072	0.628	0.103	-0.072	0.036	346
		V ₆₀₆	0.925	0.072	-0.372	0.103	-0.072	0.036	346

^a $I_{LP} = m_0 + ZP + a \times (V_{606} - I_{814}) + b \times (V_{606} - I_{814})^2$

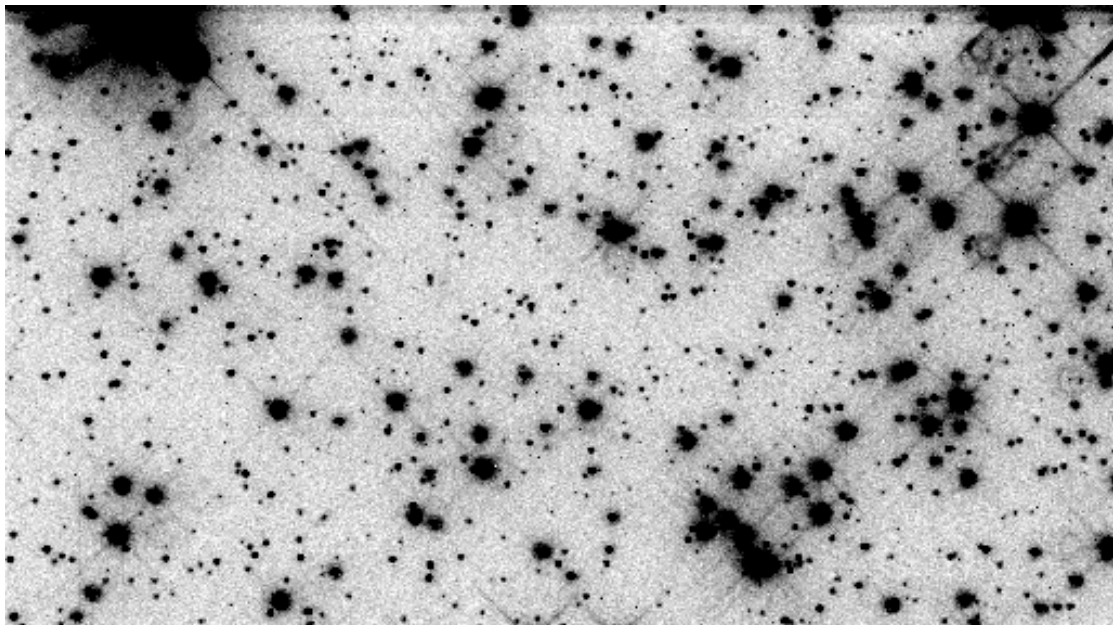


Fig. 1.— STIS LP image of 47 Tuc. The $28'' \times 51''$ field of view of the pipeline-processed STIS image of 47 Tuc, taken with the optical longpass (LP) filter, is shown; this is the image used to compute I_{LP} magnitudes of the 47 Tuc stars.

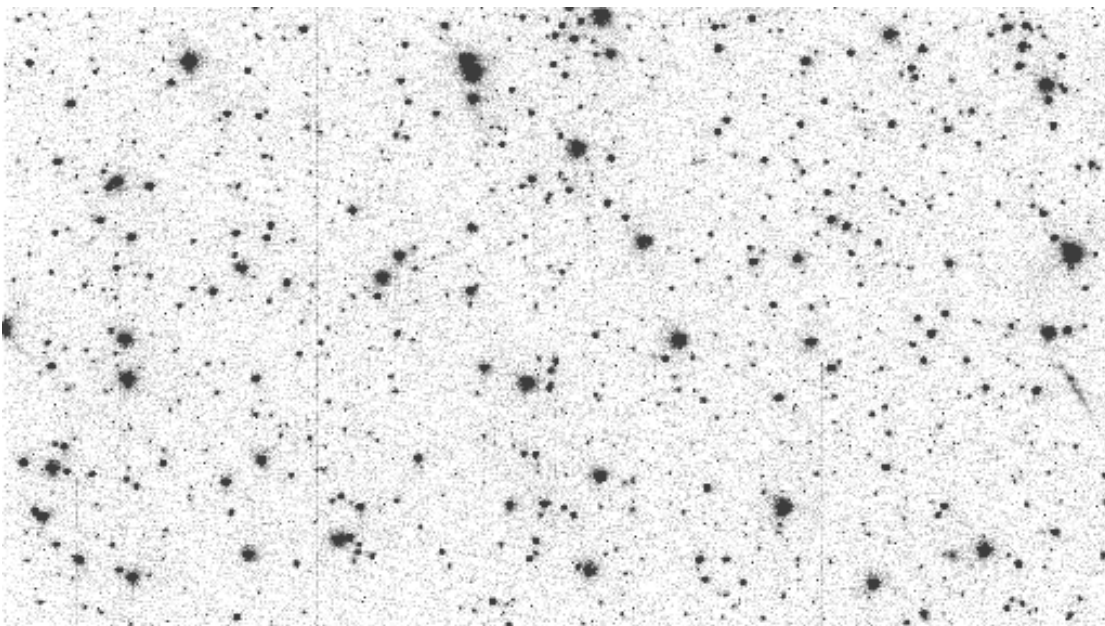


Fig. 2.— STIS LP image of M15. The $28'' \times 51''$ field of view of the pipeline-processed STIS image of M15, taken with the optical longpass (LP) filter, is shown; this is the image used to compute I_{LP} magnitudes of the M15 stars.

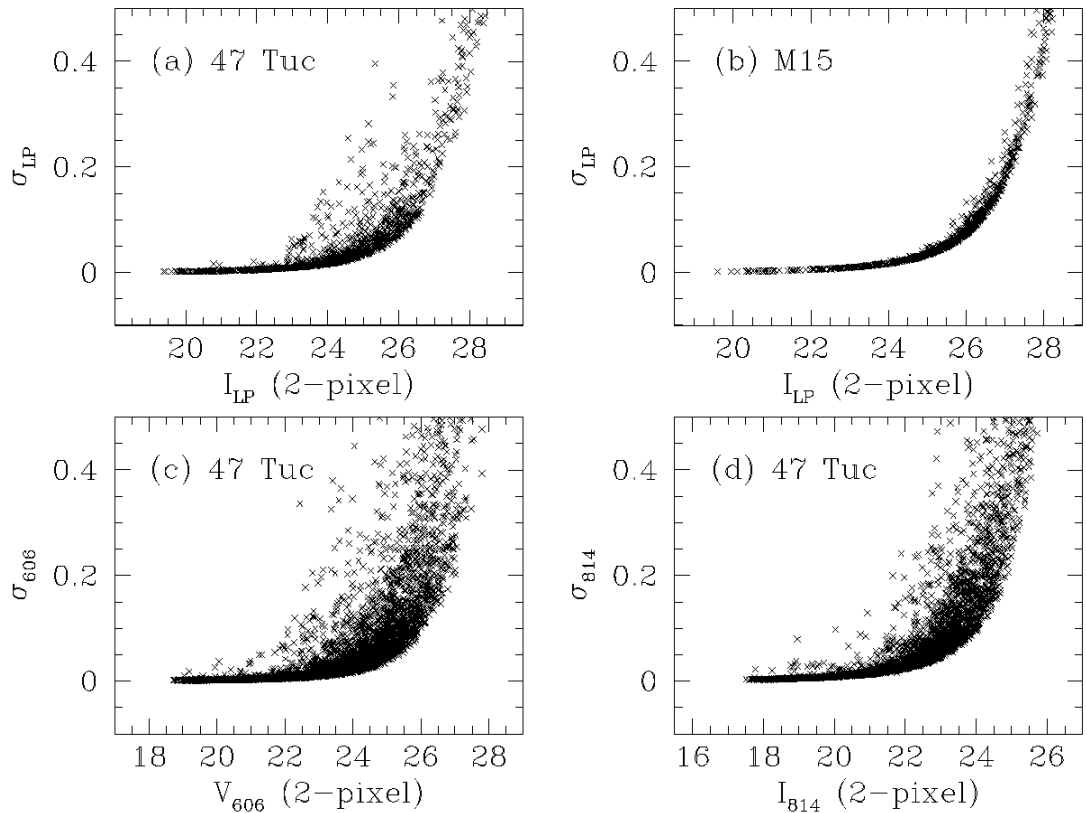


Fig. 3.— Photometric uncertainties. The 1 σ uncertainties in the 2-pixel aperture photometry are shown as a function of magnitude for (a) the STIS LP observations of 47 Tuc, (b) the STIS LP observations of M15, (c) the WFPC2 F606W observations of 47 Tuc, and (d) the WFPC2 F814W observations of 47 Tuc. The magnitudes plotted do not include the aperture or reddening corrections given in Table 2.

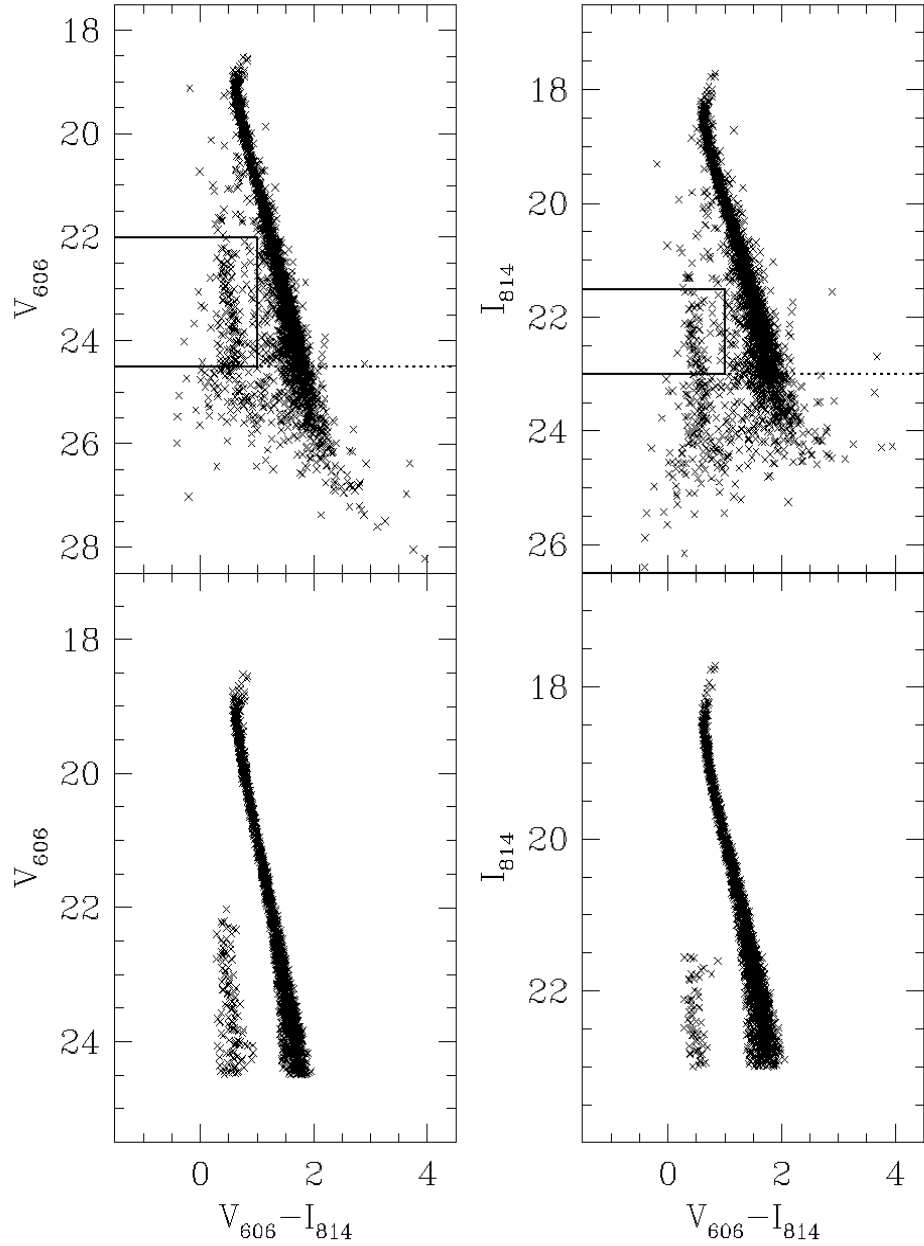


Fig. 4.— WFPC2 color-magnitude diagrams (CMDs) of 47 Tuc and the Small Magellanic Cloud (SMC). The top panels show the CMDs for the 2605 stars detected in both the F606W and F814W filters on the WFPC2 WF2 chip. Dotted lines in the top panels show the magnitude cutoffs applied before determining the cluster's main-sequence ridge lines; solid lines show the analogous color and magnitude limits applied before determining the main-sequence ridge lines for the SMC. The bottom panels show those stars determined to lie on the 47 Tuc and SMC main-sequence ridge lines, which were derived as described in the text. Reddening and extinction corrections have not yet been applied to the data plotted here.

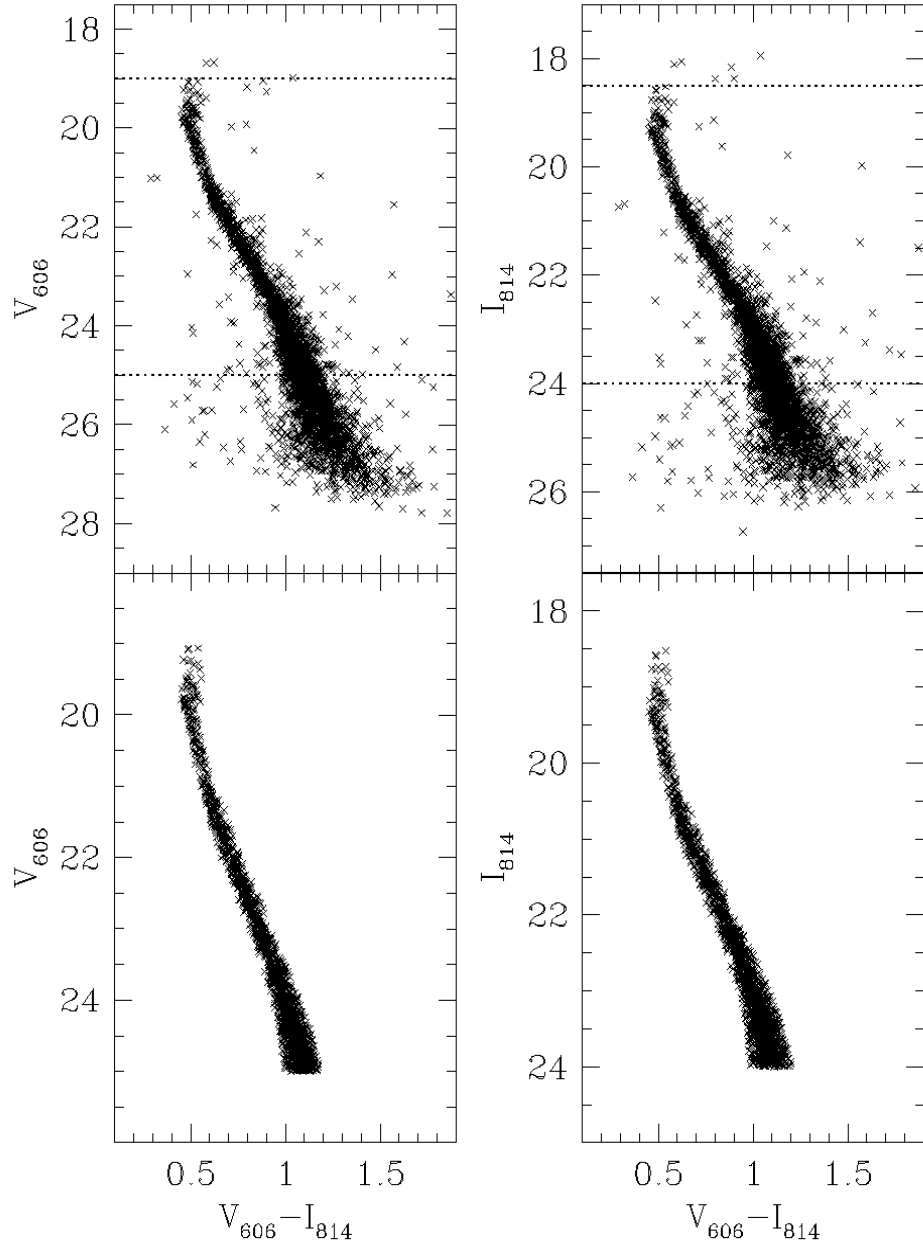


Fig. 5.— WFPC2 color-magnitude diagrams (CMDs) of M15. The top panels show the CMDs for the 3465 stars detected by Piotto, Cool & King (1997) in both the F606W and F814W filters on the WFPC2 WF4 chip. Dotted lines in the top panels show the magnitude cutoffs applied before determining the cluster's main-sequence ridge lines. The bottom panels show those stars determined to lie on the M15 main-sequence ridge lines, which were derived as described in the text. Reddening and extinction corrections have not yet been applied to the data plotted here.

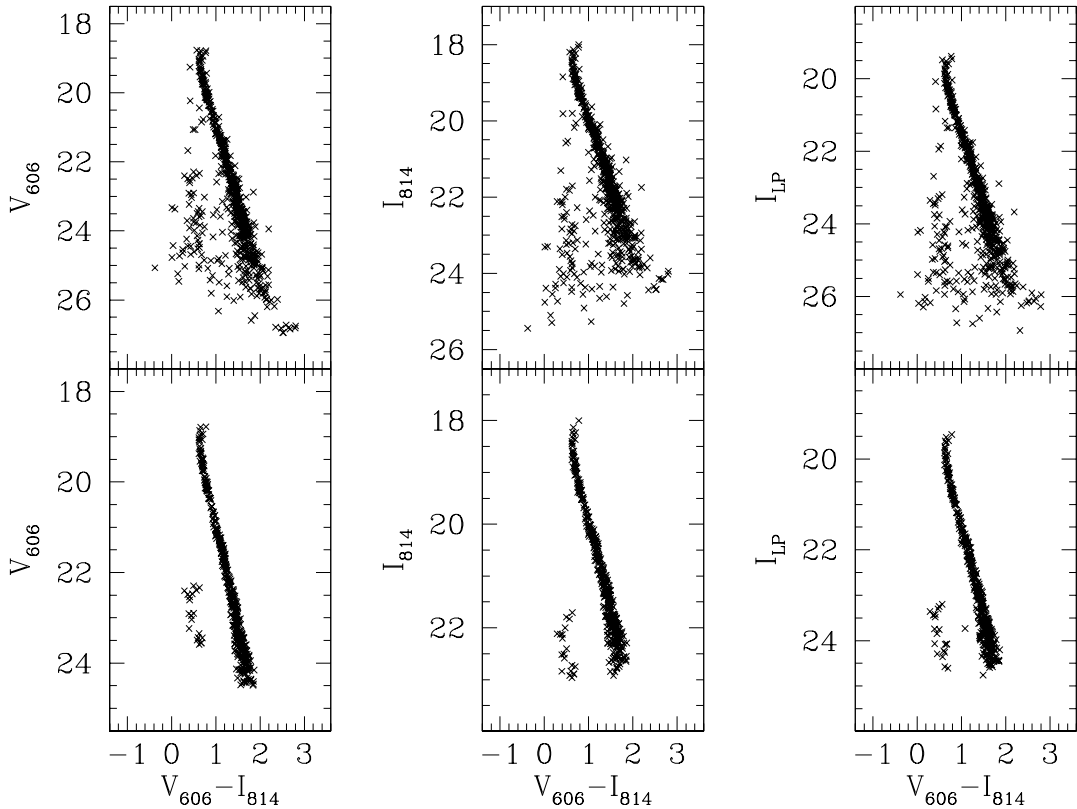


Fig. 6.— WFPC2/STIS color-magnitude diagrams (CMDs) of 47 Tuc and the Small Magellanic Cloud (SMC). The top panels show the CMDs for the stars detected in both the F606W and F814W filters of WFPC2 and in the LP filter of STIS. The bottom panels show the subsets of stars from the corresponding top panels which also lie on the WFPC2 main-sequence ridge lines of 47 Tuc and the SMC (see Fig. 4). Reddening and extinction corrections have not yet been applied to the magnitudes and colors plotted here.

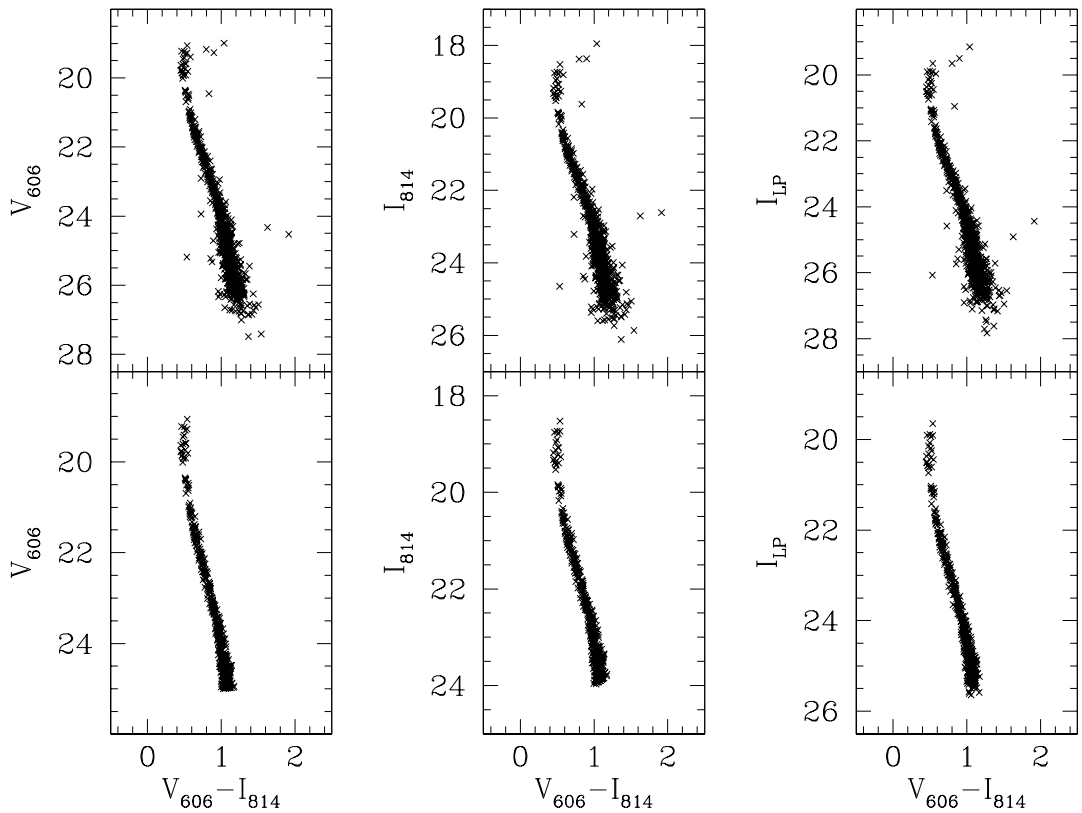


Fig. 7.— WFPC2/STIS color-magnitude diagrams (CMDs) of M15. The top panels show the CMDs for the stars detected in both the F606W and F814W filters of WFPC2 and in the LP filter of STIS. The bottom panels show the subsets of stars from the corresponding top panels which also lie on the WFPC2 main-sequence ridge lines of M15 (see Fig. 5). Reddening and extinction corrections have not yet been applied to the magnitudes and colors plotted here.

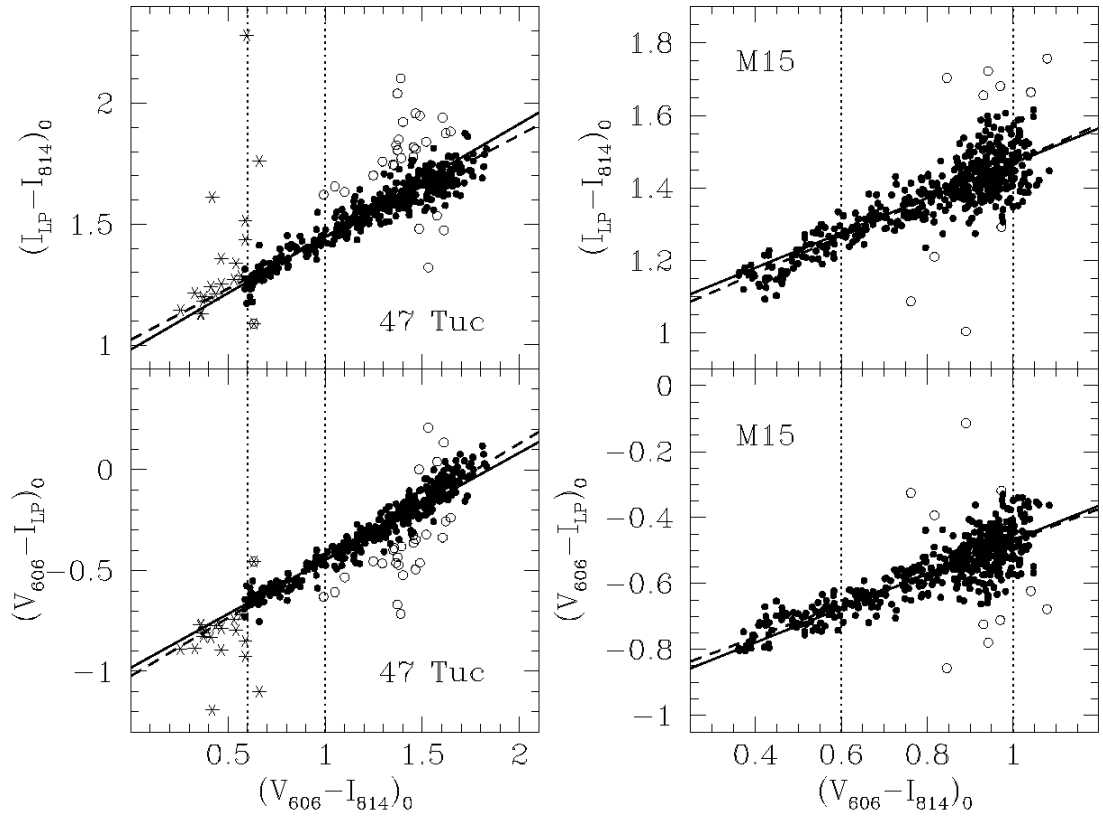


Fig. 8.— Color-color plots of 47 Tuc/SMC and M15. The left-hand panels show the 47 Tuc and SMC stars plotted in the bottom panels of Fig. 6 as circular points and asterisks, respectively, and the right-hand panels show the M15 stars plotted in the bottom panels of Fig. 7. The dashed relations in the left-hand and right-hand panels are the linear, least-squares fits to the 47 Tuc and M15 data, respectively, using iterative 3σ rejection; the open points are those rejected during the fitting. The solid lines are the analogous relations which result when only the data between the vertical, dotted lines ($0.6 \leq (V_{606} - I_{814})_0 \leq 1.0$) are used in the fitting. Coefficients of the fits are given in Table 3.

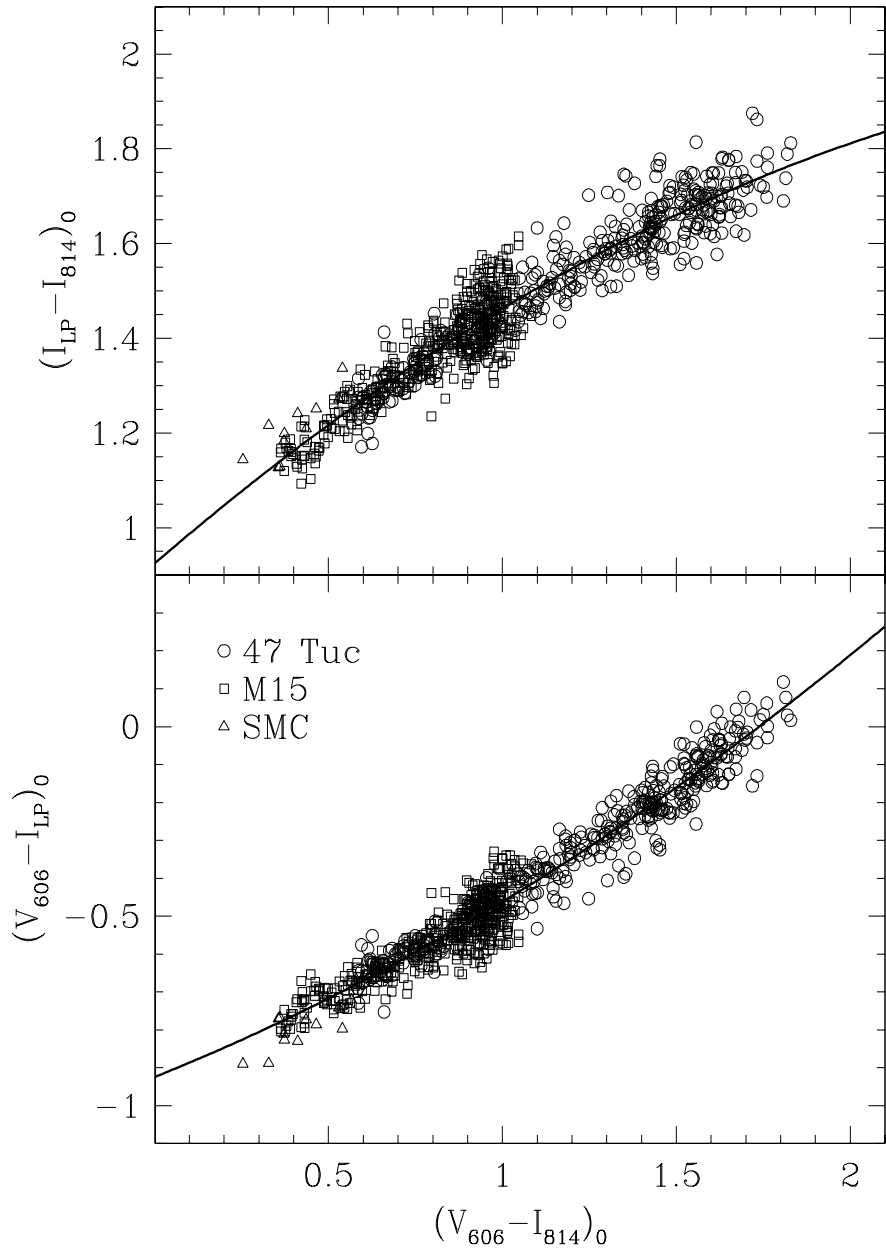


Fig. 9.— The WFPC2-to-STIS transformations. The main-sequence ridge-line stars of 47 Tuc, M15 and the SMC are combined to derive the transformations between the STIS I_{LP} magnitudes and the WFPC2 V_{606} and I_{814} magnitudes. Stars from 47 Tuc are plotted as circles, those from M15 are shown as squares, and SMC members are represented by triangles. The solid curves are the quadratic, least-squares fits to the data, using iterative 3- σ rejection; for clarity, points rejected during the fitting are not shown. The coefficients of the transformation relations are given in Table 3.

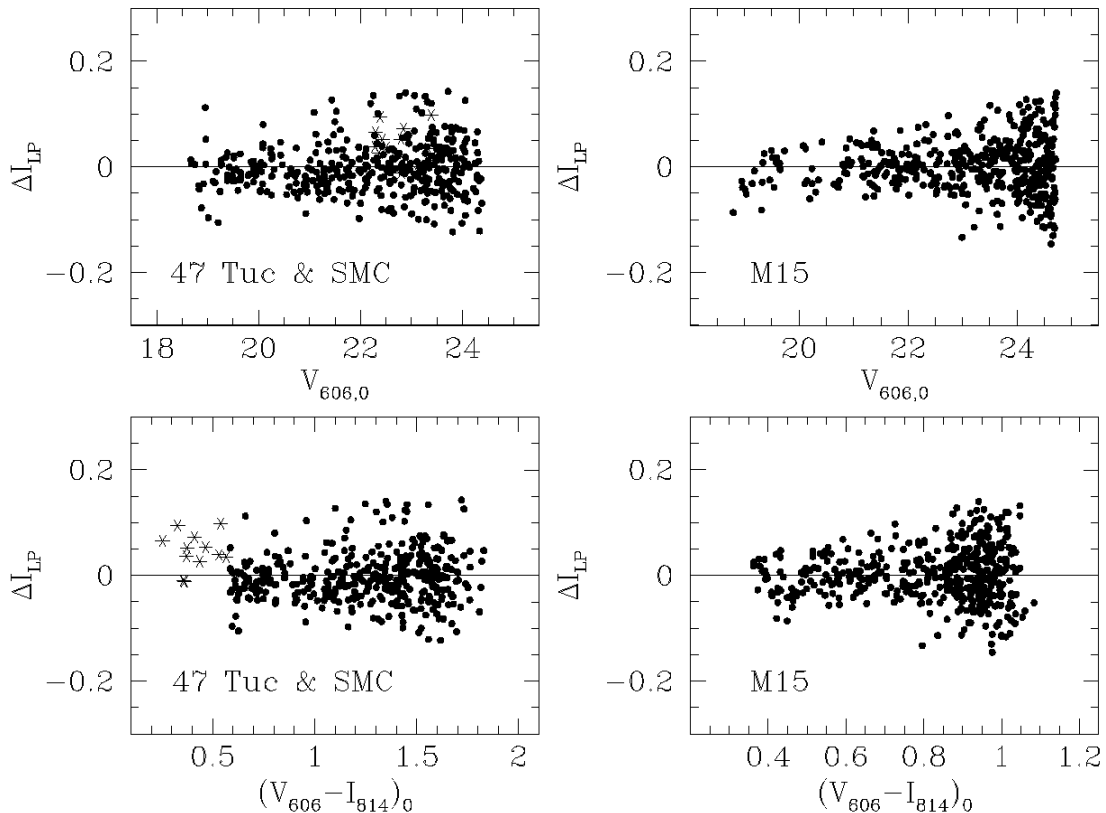


Fig. 10.— Differences between the predicted and observed $I_{LP,0}$ magnitudes. ΔI_{LP} is the difference between the observed $I_{LP,0}$ magnitude of a star and that predicted from its WFPC2 $V_{606,0}$ magnitude and its $(V_{606} - I_{814})_0$ color though the transformation shown in the bottom panel of Fig. 9. The left-hand panels show stars in 47 Tuc (filled points) and the SMC (asterisks), and the right-hand panels show M15 stars.

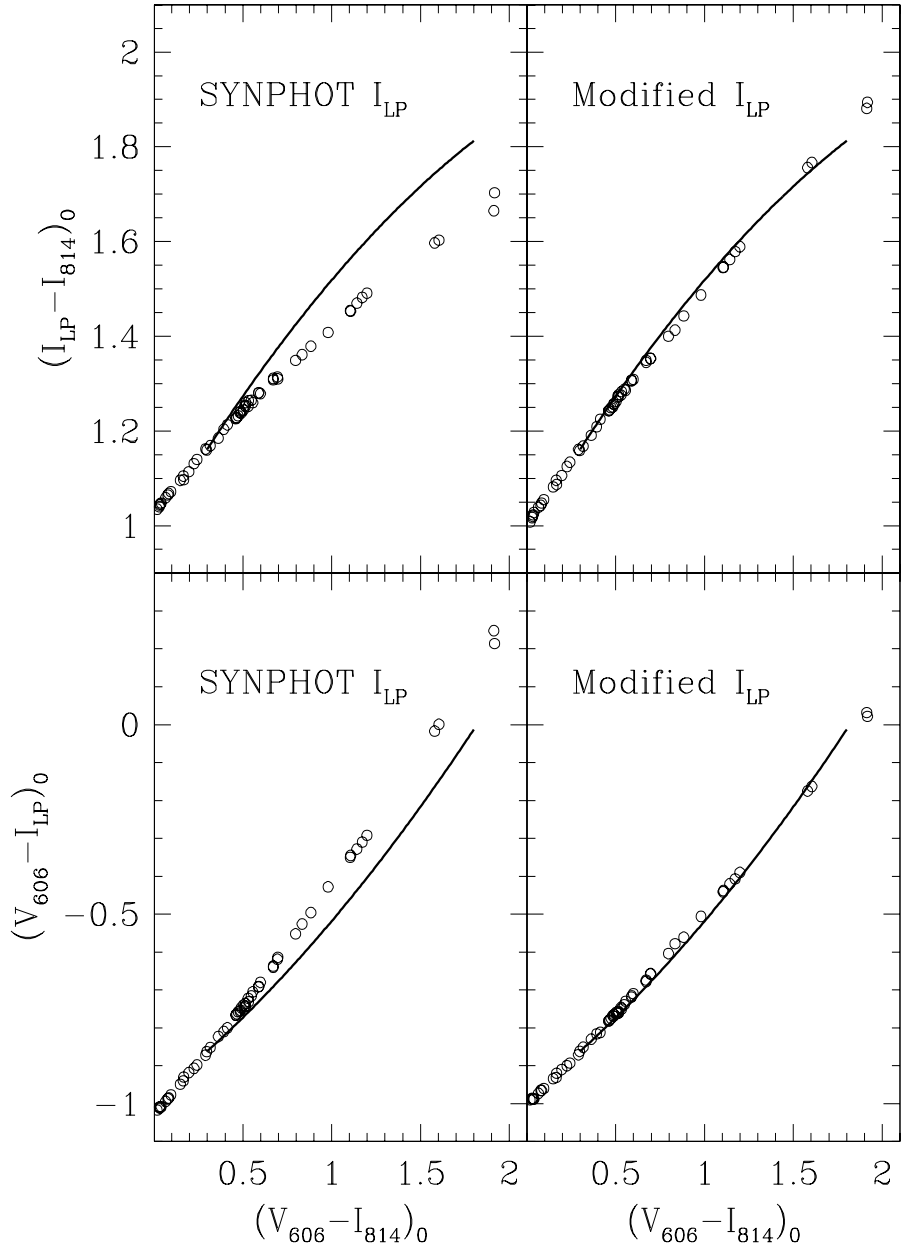


Fig. 11.— Transformation relations from SYNPHOT. The solid lines in all panels are the final transformation relations derived here (see Figure 9 and Table 3), truncated at the approximate color limits of the data used to derive the relations; the open points are the calculated SYNPHOT colors of dwarf stars in the BPGS Spectrophotometric Atlas. The SYNPHOT data in the left-hand panels has been calculated using the default SYNPHOT STIS longpass (LP) filter response function (Leitherer et al. 2000), while the STIS LP filter response suggested by Bessell (2000, private communication) was used to calculate the SYNPHOT colors shown in the right-hand panels. The SYNPHOT data and the transformation relations have been normalized at $(V_{606} - I_{814})_0 = 0.3$.

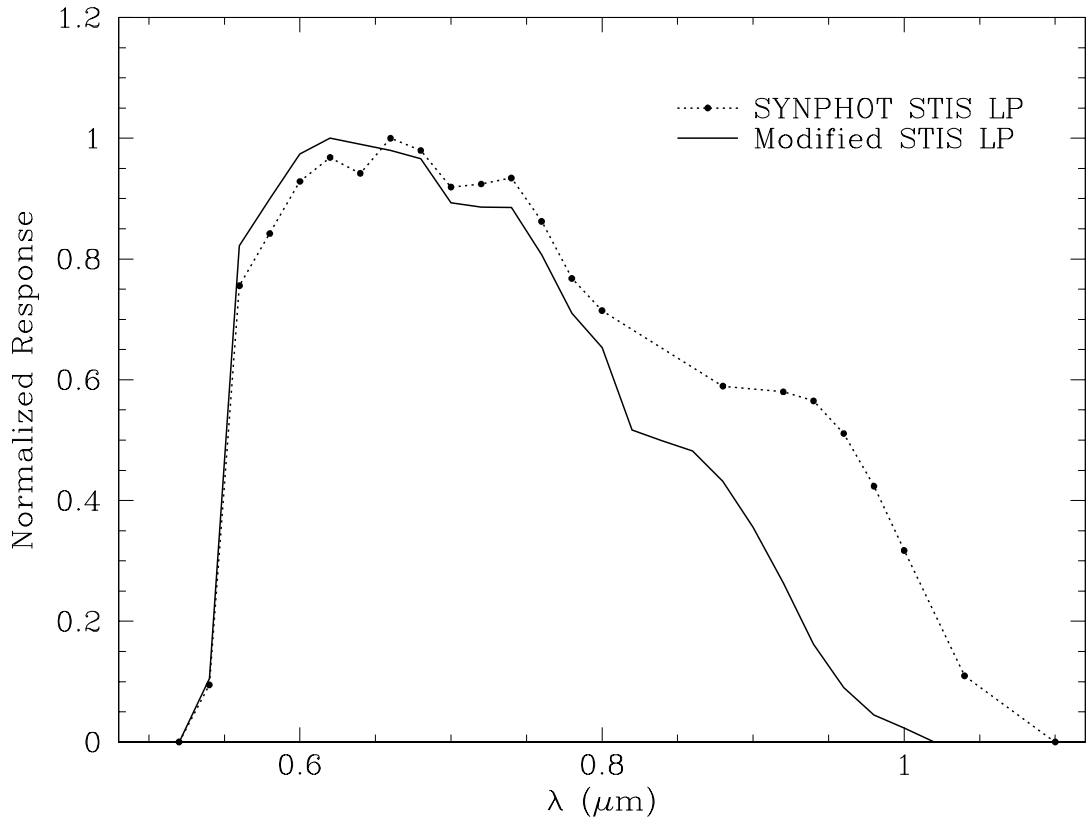


Fig. 12.— STIS LP filter response functions. Response is defined as $\lambda \times$ throughput. The dotted line is the normalized response of the STIS longpass filter given in The STIS Instrument Handbook for Cycle 10 (Leitherer et al. 2000) and used in SYNPHOT; the solid line is the normalized response of the modified STIS LP filter suggested by Bessell (2000, private communication).

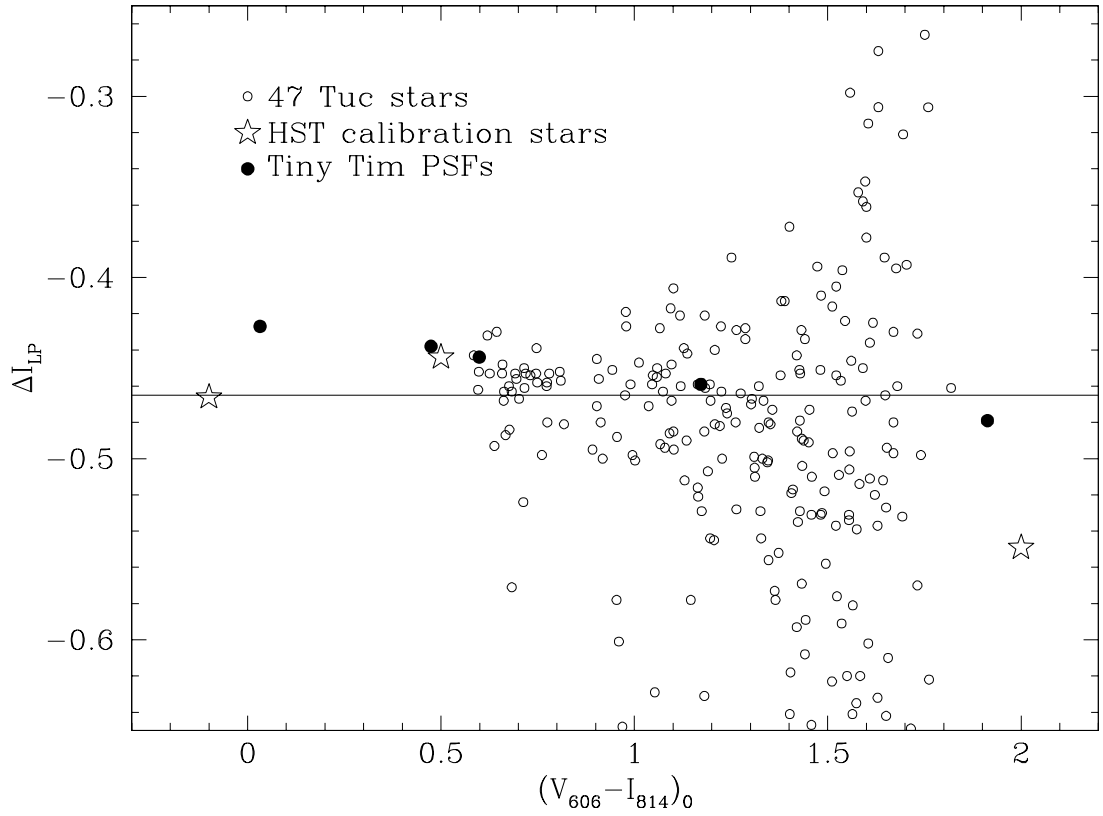


Fig. 13.— Aperture corrections as a function of color. Aperture corrections are shown for stars in 47 Tuc (open circles) that were part of the sample used to derive our empirical transformations, STIS calibration stars (filled circles), and Tiny Tim PSFs (asterisks). From blue to red, the HST calibration stars are GRW +70 5824, a white dwarf, CPD -60 7585, an F8 star, and BD -11 3759, an M4 star, and the Tiny Tim PSFs represent dwarf stars having spectral types A0, F8, G8, K7, and M3. ΔI_{LP} is the aperture correction required to transform a 2-pixel ($0.^{\prime\prime}1$) magnitude into a magnitude measured in a $0.^{\prime\prime}5$ aperture; the horizontal line shows the corresponding aperture correction applied to our 2-pixel magnitudes of 47 Tuc stars (see Table 2).